Desalination and Water Treatment
www.deswater.com
doi: 10.5004/dwt.2023.29361

287 (2023) 155–166
March

Green synthesis of sand-bimetallic Fe/Pb nanoparticles as an environmentally sustainable composite for ciprofloxacin and copper removal from aqueous solutions

Noor Alaa Abdulhusain, Ziad Tark Abd Ali*

Department of Environmental Engineering, College of Engineering, University of Baghdad/Iraq,
emails: z.teach2000@yahoo.com (Z.T. Abd Ali), noor.hussein2011d@coeng.uobaghdad.edu.iq (N.A. Abdulhusain)

Received 14 September 2022; Accepted 29 January 2023

ABSTRACT

In this study, the quartz sand (QS) was supported by the nanoparticles of Fe/Pb that were made using an *in-situ* green synthesis technique. using *Punica granatum* (pomegranate) peel extract to produce a QS-Fe/Pb nanocomposite, it utilized for the removal of ciprofloxacin (CIP) and copper (Cu(II)) from aqueous solutions in batch mode. The characterization of this composite was determined using many tests including X-ray diffraction, Fourier-transform infrared spectroscopy, scanning electron microscopy, energy-dispersive X-ray, transmission electron microscopy, and surface area. The factors that influence the removal process and achieve a removal percent of 99% were studied, and the Freundlich and Langmuir isotherm models were used to explain the sorption data, while the three kinetic models were used to determine the sorption kinetic (pseudo-first-order, pseudo-second-order, and intraparticle diffusion). The results showed that the Freundlich and pseudo-second-order models fit the experimental data more accurately. According to the reusability investigation, the CIP and Cu(II) elimination percent was greater than 60% and 50% for CIP and Cu(II) till the fifth cycle. Finally, this work may paves the road for the treatment of wastewater contaminated with different contaminants using innovative green composites created from fruit waste.

Keywords: Green synthesis; QS-Fe/Pb nanocomposite; Ciprofloxacin; Copper; Adsorption

1. Introduction

Large amounts of antibiotics are utilized nowadays because they are exceedingly successful in treating a wide range of bacterial infections in humans, animals, poultry, and fish. Ciprofloxacin (CIP) is a sort of antibiotic that is commonly used as a treatment for a variety of bacterial infections around the world [1–3]. Fluoroquinolones are a type of broad-spectrum antibiotic that is commonly used in human and veterinary medicine. Today's most popular fluoroquinolone is a second-generation drug called CIP [4], while copper (Cu(II)) is a vital component of the heavy metal industry, with widespread use in plating, petroleum refinement, the manufacturing of brass, and Cu-based pesticides [5,6], The residues of mining, smelting, and other processes used to process copper ore also release copper into the environment. It causes a variety of developmental defects and illnesses in humans [7]. The most common form of environmental pollution in the world is a mixture of organic chemicals and heavy metals, so thinking about the process of removing these contaminants in efficient ways has become an urgent need to ensure a clean environment for humans [8,9].

Adsorption is one of the primary procedures for removing antibiotics or heavy metal contaminants from aqueous systems. This method is appealing for treating emerging contaminants due to its low operating costs, simplicity of use, ease of sorbent regeneration, and low environmental toxicity [10]. The researchers have investigated a number

* Corresponding author.

of low-cost sorbents including magnetic nanocomposite, metal–organic frameworks, graphene oxide, composites based on clay, and materials made from agricultural and industrial waste [11,12].

The wastewater remediation processes have seen encouraging results from the nano zero-valent iron (nZVI) technology. The nZVI has limitations, though, including quick aggregation, poor stability, and ineffective separation from the reactants. In order to address these areas, the nZVI particles are typically improved in a number of ways [13], including emulsifying nZVI particles, doping with an additional metal, applying a chemical stabilizer to the surface, and adding support material. Cu, Ag, Pt, Ni and Pd are a few of the noble metals that are doped into nZVI in small amounts for the production of bimetallic nZVI particles [14,15]. These metal dopants function as catalysts, promoting the ability of the nZVI particles to remove contaminant [16,17]. The dopant metal stabilizes the system by preventing the oxidation of airborne particles in addition to acting as a catalyst. Additionally, it assists in reducing the activation energy, enhancing the reduction energy [18] and also stimulates H_2 production near the surface of nZVI, which increases the reactivity of iron NP [19].

Through a survey of the previous literature, no one was found to employ Pb(II) as a dopant metal, that was used in this work for the first time, and other studies used harmful and dangerous compounds like borohydride to create nanoparticles, which might potentially make the environment more toxic overall [19–21] .The fruit's peel, which contain the necessary bio-organics for the process, could be used to biosynthesize the nanoparticles as a potential solution. Pomegranates have a variety of biologically active substances, which is why they have been used as a medicine for a long time. Its extract has greater antioxidant activity than pomegranate seed and pulp. Due to the peel extract's high polyphenolic content, which may be used to create nanoparticles, it has a reducing ability [22]. Therefore, pomegranate peel extract was used for the current study's Fe/Pb nanoparticle synthesis. Fe/Pb nanoparticles would be quite expensive to utilize directly in commercial applications, and using the bare nanoparticles to remove contaminants would prevent the regeneration and reuse of the reactant. An inert substrate or support system for the particles can be offered to overcome these restrictions. The sand was utilized as an inert and supporting material to immobilize the Fe/Pb nanoparticles because it is an inert substance that provides excellent support because surface particles create fine layers on the sand surface [23].

The main objective of the present study is to produce a novel adsorbent that can remove CIP and Cu(II) from aqueous solutions. There have been no instances in the literature where the use of the Pb with nZVI supported on the sand to produce QS-Fe/Pb in a green method has been used for the removal of CIP and Cu(II) from the aqueous medium. However, The following points were used to accomplish this objective of the current work: (1) manufacturing the QS-Fe/Pb nanocomposite in a green method as an alternate method for chemical synthesis by using pomegranate peels extract, the pomegranate peels were used to facilitate green synthesis, which reduces the production of domestic waste and avoids employing hazardous chemical reducing agents, (2) studying the ability of this nanocomposite to remove CIP and Cu(II) from aqueous solutions, (3) determining the characterization of the nanocomposite using different tests, and (4) reusability tests up to five cycles were also performed to confirm the applicability and efficiency of the fabricated nanocomposite. Finally, *in-situ* green synthesis of Fe/Pb nanoparticles on quartz sand (QS-Fe/Pb) and their use as a sorbent in the current work is considered to be among the most promising studies in the field of production of new, low-cost, and efficient adsorbents.

2. Materials and methods

2.1. Materials

Quartz sand (QS) supports as the matrix that is supported and immobilized, was purchased from the local market (Al-Nawafeth Company), its initial porosity = 0.45, particle size range = 0.3–0.5 mm, and specific gravity = 1.363. The ferric chloride ($FeCl_3$) anhydrous iron(III) chloride, lead sulfate ($PbSO_4$), copper(II) nitrate trihydrate ($Cu(NO_3)_2{\cdot}3H_2O$), and absolute ethanol (99.9%) were purchased from local market)Honeywell Specialty Chemicals, Germany(, while and ciprofloxacin ($C_{17}H_{18}FN_3O_3$) from Samarra Pharmaceuticals Factory, Iraq. All chemicals and reagents were analytical grade.

2.2. Preparation of contaminated aqueous solutions

The synthetic solutions of Cu(II) and CIP with a concentration of 1,000 mg/L were prepared by dissolving 3.929 and 1 g of copper nitrate trihydrate and ciprofloxacin, respectively, in 1 L of distilled water. The required contaminant concentration is obtained through the dilution process. The pH of the synthetic solutions was set using 0.1 M of HCL or NaOH as needed.

2.3. Synthesis of QS-Fe/Pb nanocomposite

In order to prepare the pomegranate peel extraction using ethanol, the pomegranate fruit was purchased from a local seller, the fruits were cleaned with tap water and peeled by hand. The peels were dried for 40 h at 60°C in an oven, then extracted (10%) with 100% ethanol in a shaking incubator for 24 h, then the mixture was filtered using Whatman No 1 Filter Paper. Finally, the supernatant was collected and kept at 20°C for future use. The green synthesis of the QS-Fe/Pb composite was done according to the method cited by the study of Ravikumar et al. [23]. Depending on this method, a screw-capped bottle was filled with 100 g of QS, to which 150 mL of 0.1 M $FeCl_3$ solution was gently added. The screw-capped bottle was then placed on an orbital shaker for 30 min to ensure that the $FeCl_3$ solution and QS were homogenously mixed. The Fe-coated sand was then dried overnight in an 80°C vacuum oven. The ethanolic extract (10%) of pomegranate peel was gently added to the dried $FeCl_3$-coated sand at room temperature (29°C). During the process, the color of the mixture changed from golden yellow to black. The development of nano zero-valent iron nanoparticles is indicated by the appearance of black precipitate as mentioned in other works Gopal et al.

[17]. The mixture was maintained on an orbital shaker for 30 min at room temperature after adding the pomegranate peel extract for uniform mixing. The shaking time was increased to 1 h after adding 150 mL of 0.1 M $PbSO_4$ solution to this mixture, after that, the prepared QS-Fe/Pb composite was filtered through a Whatman No 1 Filter Paper before being washed three times with 100% ethanol and dried in an 80°C vacuum oven, then it was kept in a closed container for using in the next experiments. The schematic diagram of the green synthesis of QS-Fe/Pb nanocomposite is illustrated in Fig. 1.

2.4. Characterization of QS-Fe/Pb composite

The created composite (QS-Fe/Pb) underwent a number of analyses at the University of Tehran, College of Science, Iran before being utilized in the experiments to investigate various elements of its properties, as follows:

2.4.1. X-ray diffraction analysis

The synthesized QS-Fe/Pb composite's crystallinity was verified using the X-ray diffraction (XRD) analysis.

2.4.2. Fourier-transform infrared spectrometry analysis

This test was used to determine the functional groups on the surface of the active substance that were liable for the contaminants removal.

2.4.3. Surface area

A surface area analyzer was used to quantify the specific surface area, which is an essential component in determining how effective adsorbent materials are. This was done using the Brunauer–Emmett–Teller method, which relies on nitrogen adsorption at 77 K.

2.4.4. Scanning electron microscopy/energy-dispersive X-ray analysis

Scanning electron microscopy (SEM) was used to investigate the morphology of QS and QS-Fe/Pb composites, while the energy-dispersive X-ray (EDX) analysis was used to recognize the elemental composition of the prepared composite.

2.4.5. Transmission electron microscopy

The morphology of the QS and QS-Fe/Pb composite were examined using a Morgagni 270-D transmission electron microscope and an 80.0 kV speed voltage. To estimate the transmission electron microscopy (TEM), the samples were drawn by dabbing a drop of the sample solution onto the Formvar® coated grids.

2.5. Batch and experiments

The optimum batch conditions for the removal of the contaminants were identified by performing batch studies

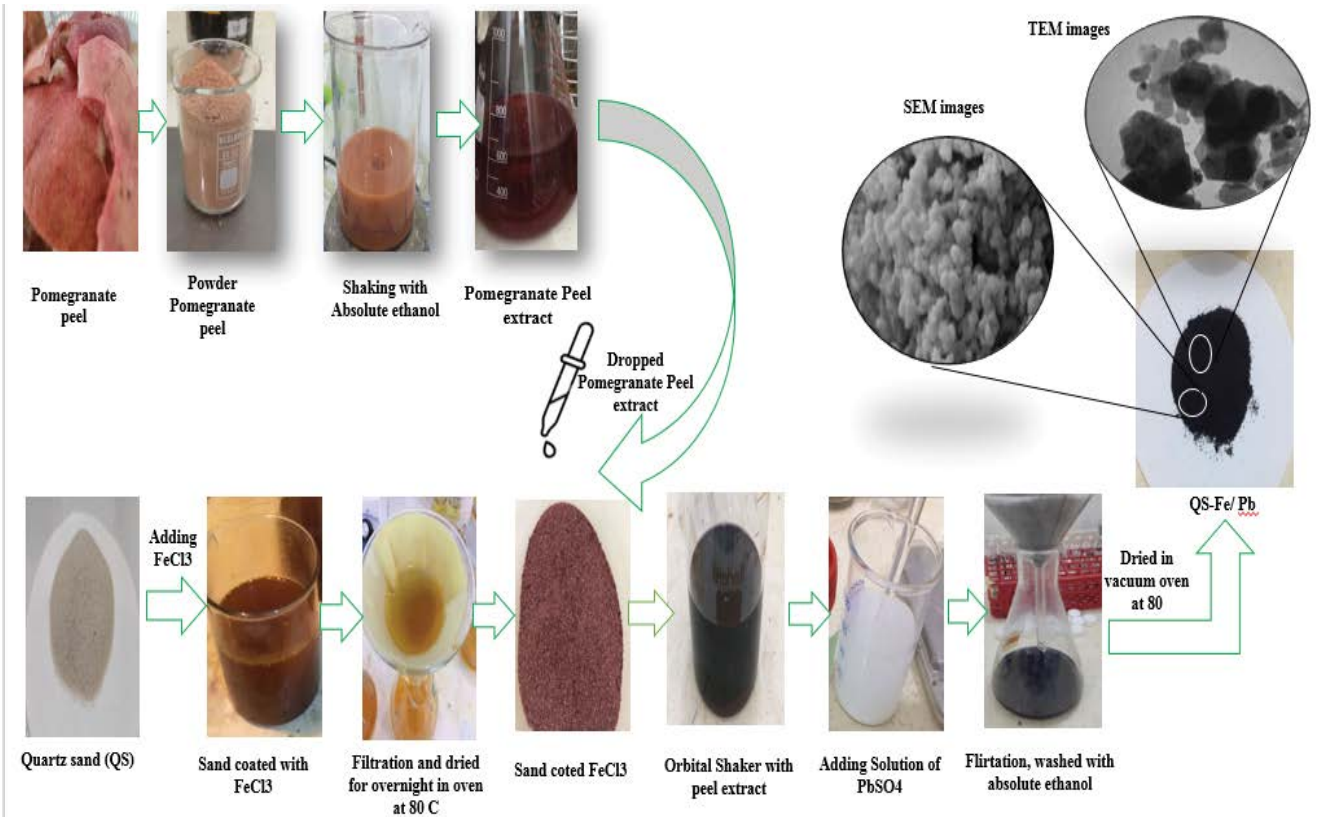

Fig. 1. Schematic diagram of the green synthesis of QS-Fe/Pb nanocomposite.

to the CIP and Cu sorption equilibrium data. These conditions including many variables such as contact time, pH of the initial solution, agitation rate, concentration of the initial contaminants, and dosage of QS-Fe/Pb. The following procedure was used in the experimental work: each 250 mL flask was first filled with 50 mL of the CIP and Cu(II) solutions at a concentration of 50 mg/L, and then 0.2 g of the prepared composite was added. After being stirred for 3 h at 200 rpm, all of the flasks containing the adsorbent, as well as the CIP and Cu contaminant solutions, were filtered to separate the clear contaminant solution from the remaining solid material, the residual untreated quantity of the CIP and Cu present in the solution was specified using 10 mL samples drawn from the filtered solution. Cu(II) was examined using atomic absorption spectroscopy, and the CIP was evaluated using UV-Visible spectroscopy, to guarantee the accuracy of the findings, every sample was re-examined three times. At various pH ranges (for CIP pH = 2–12 and for Cu(II) pH = 2–7). Based on the various initial concentrations of the contaminants (C_0, 50–250 mg/L), the sorption was calculated using a variety doses (0.05–1 g/50 mL), time range from 0 to 180 min. In order to adopt the best experimental results, Eqs. (1) and (2) were actually used to calculate the removal percent (R%) and amount of the contaminants retained in the solid phase (q_e) [24,25].

$$R\% = \frac{C_0 - C_t}{C_0} \times 100 \tag{1}$$

$$q_e = \frac{C_0 - C_e}{m} V \tag{2}$$

where C_0 and C_e, initial and equilibrium contaminants concentrations (mg/L) in the flask, V is the volume of the solution in the flask (L), and m is the mass of the QS-Fe/Pb composite in the flask (g).

2.6. Isotherm models

Two isotherm models were used to depict the sorption data:

2.6.1. Freundlich model

Useful for non-homogeneous surfaces with multi-layer sorption, it has the following formula [26]:

$$q_e = K_F C_e^{1/n} \tag{3}$$

where K_F is the Freundlich constant and $1/n$ (<1) represents the sorption intensity.

2.6.2. Langmuir model

This model was provided in the following equation below, and is used for homogenous surfaces and monolayer sorption [27]:

$$q_e = \frac{q_{\max} b C_e}{1 + b C_e} \tag{4}$$

where $q_{\max}$ denotes the maximum adsorption capacity (mg/g) and b denotes the intensity of the contaminant onto the solid phase.

2.7. Kinetic models

The solid-aqueous solution interface in the boundary system is regulated by the residence duration of pollutants that have been eliminated as a result of the sorption process's kinetics, which clarifies the absorption rate of solute particles [28]. This rate can be calculated with the following models:

- Pseudo-first-order model: The following expression can be used to estimate the sorption rate over time [29,30]:

$$\frac{dq}{dt} = k_1 \left(q_e - q_t \right) \tag{5}$$

Eq. (5) is integrated to obtain Eq. (6):

$$q_t = q_e \left(1 - e^{-K_1 t} \right) \tag{6}$$

where q_e is the quantity of solute (mg/g) adsorbed at equilibrium, q_t is the quantity of solute (mg/g) adsorbed at a specific time t, and K_1 is the rate constant (min^{-1}) for pseudo-first-order kinetic model at equilibrium.

- Pseudo-second-order rate equation: The contaminated monolayer is fixed to the sorbent surface, the sorbent has an identical sorption energy, and there is no interaction between the contaminant sorbed molecules. These assumptions can be expressed by the ordinary differential equation that follows [31].

$$\frac{dq}{dt} = K_2 \left(q_e - q_t \right)^2 \tag{7}$$

where K_2 is the rate constant of the second model (g/mg·min). Eq. (8) is integrated to produce the second equation in nonlinear forms.

$$q_t = \frac{t}{\left(\frac{1}{K_2 q_e^2} + \frac{t}{q_t} \right)} \tag{8}$$

Because pseudo-first-order and pseudo-second-order models are insufficient to explain the dominating processes, the following intraparticle diffusion has been employed:

3. Intraparticle diffusion

$$q_t = K_{\text{int}} t^{0.5} + C \tag{9}$$

where K_{int} is the diffusion model's sorption rate constant (slope) (mg/g·$min^{0.5}$) and C is the intercept and indicates the boundary layer's thickness.

4. Results and discussion

4.1. Characterization of the prepared composite (QS-Fe/Pb)

4.1.1. XRD analysis

The XRD spectral data for QS-Fe/Pb composite before and after interaction with Cu and CIP is illustrated in Fig. 2. This figure indicates prominent diffraction peaks at 2θ = 42.775°, 50.475°, 60.325°, and 68.475°, which clearly signifies the formation of Fe/Pb nanoparticles on the sand surface [32]. The peak (60.325) intensity significantly decreased after interaction with CIP due to the redox reaction between CIP and QS-Fe/Pb. These reflections represent the new sites created on the sand surface that converted the inert sand to reactive material [33], while the decrease just after the interaction of QS-Fe/Pb with Cu in the peak (75.975). The difference in the crystallinity and phase of the QS-Fe/Pb during the chemisorption of Cu may explain the XRD shapes of the material before and after adsorption.

4.1.2. Fourier-transform infrared spectroscopy analysis

The Fourier-transform infrared spectroscopy (FTIR) spectral analysis of QS-Fe/Pb in a range of 400–4,000 cm^{-1} is given in Fig. 3. The stretching vibrations of the O–C–O and C = C functional groups, which are seen as many peaks at 2,351; 2,150, and 1,632 cm^{-1}, are directly related to the pomegranate peel extract's polyphenol content [34]. The findings obviously show that the bio-organics in the fruit peel extract caused the Fe/Pb to accumulate on the sand. This is also supported by prior research on the production of Fe–Ni particles using pomegranate peel extract [18]. FTIR spectrum measurements support the adsorption of Cu(II) and CIP by QS-Fe/Pb (Fig. 3). The peaks at 3,416; 1,874, and 1,156 cm^{-1} for CIP and 3,416 and 1,095 cm^{-1} for CU confirm the existence of adsorbed CIP and Cu(II) on the surface of QS-Fe/Pb [18].

4.1.3. Surface area

The surface area of QS-Fe/Pb (6.0488 m^2/g) was appreciated to be significantly high than it was with QS. (0.56233 m^2/g). Sand had a pore volume of 0.003829 cm^3/g, which was increased to 0.008355 cm^3/g after being coated with nanoparticles. The increase in QS-Fe/Pb surface area and pore volume may be due to the coating of nanoparticles on the surface of the sand. The outcome of this test matched the findings of other researchers [23].

4.1.4. SEM/EDX analysis

The SEM images and EDX analysis of QS and QS-Fe/Pb are shown in Fig. 4. The mean diameter of QS-Fe/Pb was 56.97 nm, and the most of the particles were spherical. Furthermore, QS-Fe/Pb EDX analysis verified the presence of both Fe and Pb on the sand surface.

4.1.5. TEM analysis

Fig. 5 demonstrates the TEM images of the QS and QS-Fe/Pb composite. It is clear from Fig. 5a that the sand is made up of a single piece (particle) without any smaller constituent parts, proving that the sand surface is uncoated. The existence of these pieces demonstrates that the Fe/Pb nanoparticles were successfully deposited on the sand surface, even if Fig. 5b shows that small intermittent pieces were created (discrete particles) that are quite different from those seen in Fig. 5a.

4.2. Impact of operational conditions in batch mode

4.2.1. Contact time

The determination of the equilibrium time is a crucial step in the batch tests, the interaction time in this experiment varied from 5 to 180 min with experimental conditions is illustrated in Fig. 6A. The result showed that the highest removal percent (70% and 60%) was mainly achieved at 70 and 120 min for CIP and Cu(II), respectively. The significant increase in the CIP and Cu removal percent over time is most likely caused by the prepared composite sites that were available and assigned for the sorption of CIP and Cu; however, as these sites were reduced, the sorption rate decreased, especially after 70 and 120 min for CIP and Cu(II), respectively [35]. As a result, the elimination percent did

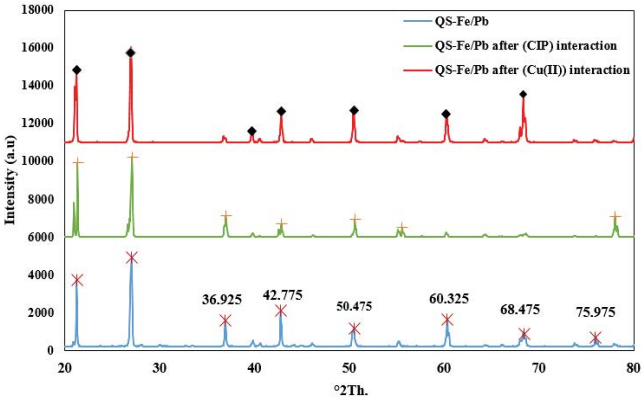

Fig. 2. X-ray diffraction test for QS-Fe/Pb before and after interaction with ciprofloxacin and Cu(II).

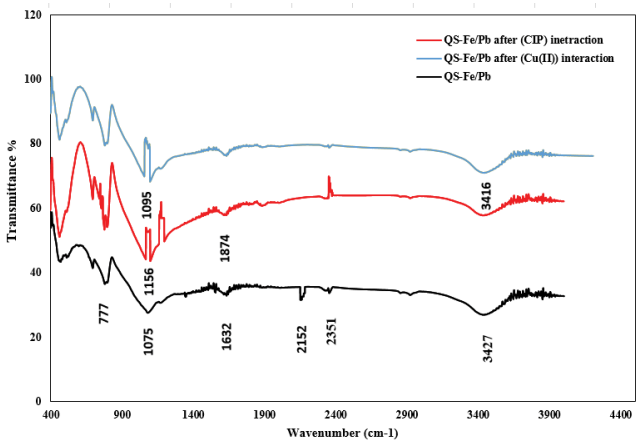

Fig. 3. Fourier-transform infrared spectroscopy analysis for QS-Fe/Pb before and after interaction with ciprofloxacin and Cu(II).

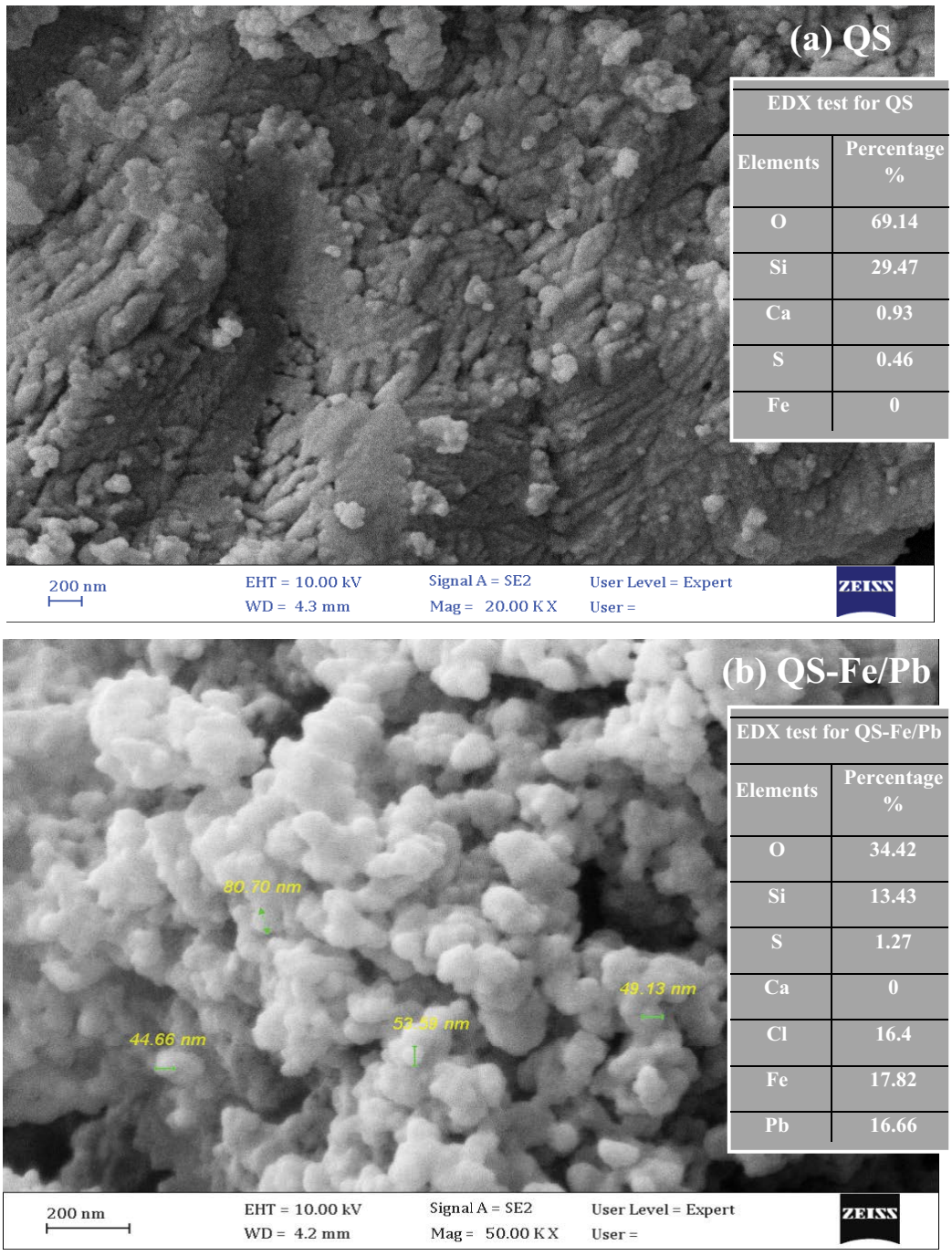

Fig. 4. Scanning electron microscopy images and energy-dispersive X-ray tests for (a) QS and (b) QS-Fe/Pb nanocomposite.

not significantly change up to 180 min before reaching the equilibrium time; therefore, 70 and 120 min, respectively, represent the optimal times to reach the equilibrium state for CIP and Cu(II).

4.2.2. Effect of initial solution pH on CIP and Cu(II) removal

The pH of an aqueous domain must also be taken into account in this study since it affects the removal of CIP and Cu(II). In order to accomplish this, tests must be carried out using fixed initial pH ranges, namely 3 to 12 for CIP and 3 to 7 for Cu(II), using operating parameter values as shown in Fig. 6B. It can be noted that there was an increase in the contaminants removal percent with increasing in initial pH value from 3 up to 7 and 6 for CIP and Cu(II), respectively, which represent the best point that achieves the highest removal percent of 74% and 60% for CIP and Cu(II), respectively, after that, the removal percent decreased with an increase in the initial value of pH. This result agreed with other works such as Liu et al. [36] .This behavior can be explained as

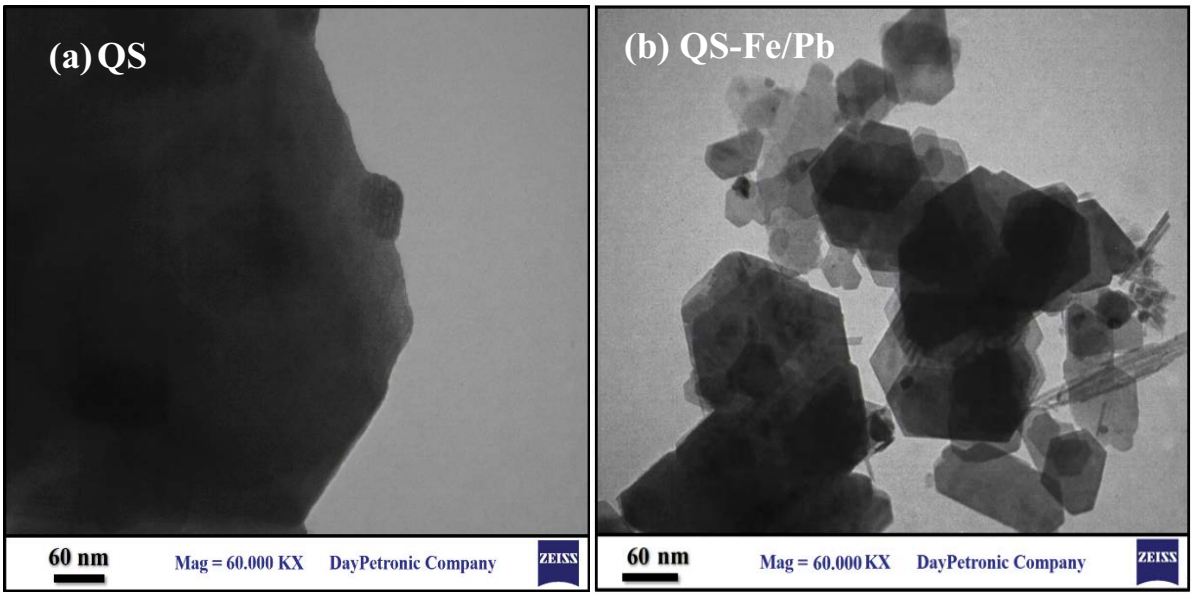

Fig. 5. Transmission electron microscopy images for (a) QS and (b) QS-Fe/Pb nanocomposite.

follows, the increasing pH values within the experimental range of 2–7 and 2–6 for CIP and Cu(II), respectively, led to an increase in the percent removal because increasing the pH value leads to a decrease in the obstacles for attractiveness between the contaminants and the active sites of the adsorbent (QS-Fe/Pb nanocomposite) by repulsion which is controlled by the protonation of the nanocomposite [17]. After that, the removal pattern was different, it was decreased with increasing the pH value up to 12 and 7 for CIP and Cu(II), respectively, due to the ionization of hydroxyl groups [37]. It is worth mentioning when assuming that the dissolved oxygen concentration (DO) was enough at the start of the reaction (removal process), the significant role in the elimination of contaminants will be Fenton-like reactions. Therefore, the following reaction occurs to nanocomposite (QS-Fe/Pb) [24]:

$$Fe_0 + O_2 + 2H^+ = Fe^{2+} + H_2O_2 \quad (10)$$

$$Fe_0 + H_2O_2 + 2H^+ = Fe^{2+} + 2H_2O \quad (11)$$

$$Fe^{2+} + H_2O_2 = Fe^{2+} + {}^{\bullet}OH + OH^- \quad (12)$$

The pH of the solution and the oxygen concentration decreased gradually because of the consumption of H^+ and O_2 and the generation of OH^-, in addition, increasing the concentrations of OH^- and Fe^{2+} after the above reactions led to precipitate of the $Fe(OH)_3$ or $Fe(OH)_2$ according to the following reaction that also assists in contaminants removal through sorption process [19]:

$$Fe^{2+} + 2OH^- = Fe(OH)^2 \quad (13)$$

$$4Fe + (OH)^2 + 2H_2O + O_2 = 4Fe(OH)^3 \quad (14)$$

4.2.3. Effect of agitation speed

The effect of the agitation speed on the removal of the Cu(II) and CIP was evaluated by changing the speed from 0 to 250 rpm, while the other parameter equal to the best ones specified previously. It is clear from Fig. 6C, that about 14% and 10% of the CIP and Cu(II), respectively, were removed prior to being shaken, and the removal percentage increased as the shaking speed increased up to 200 rpm, yielding higher removal percentages of 74% for CIP and 60% for Cu(II) after that, there was no clear increase in the removal percent when the agitation speed increased to 250, as illustrated in Fig. 6C, so, the 200 rpm was selected as the best agitation speed value for the subsequent experiments. The explanation of the results of this section depends on the fact that any rise in the agitation speed leads to an escalation in the distribution of the contaminants on the sorbent surface (QS-Fe/Pb composite). As a result, there was sufficient contact between the sorbate solution and the active sites, which aided in the sorbate solution's successful transfer to the sorbent sites [38].

4.2.4. Effect of initial concentration

Other experiments were carried out to study the effect of various initial concentrations (C_0) of CIP and Cu(II) on removal percent. These tests were conducted using C_0 ranging from 50 to 250 mg/L under operating conditions depicted in Fig. 6D. This figure clearly demonstrates the significant decrease in CIP and Cu(II) removal when their initial concentration (C_0) was elevated. The main reason for this drop in removal rates was due to the adsorbent's sites becoming saturated with the pollutants' molecules [39,40]. Based on the results of this experiment, the lowest dose utilized (50 mg/L)

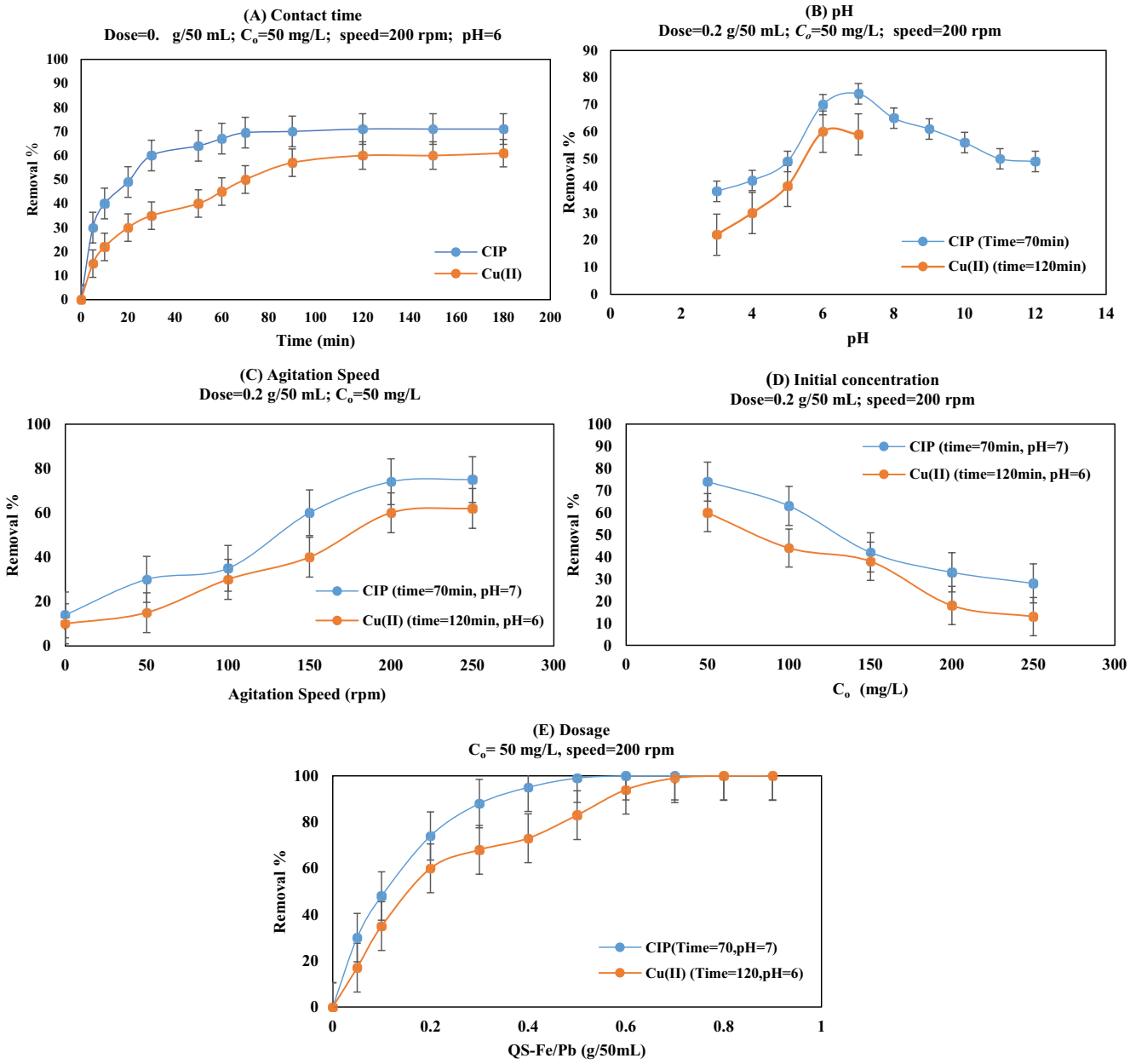

Fig. 6. Ciprofloxacin and Cu(II) removal percent at different (A) contact time, (B) pH, (C) agitation speed, (D) initial concentration, and (E) dosage of QS-Fe/Pb.

was found to be the optimal beginning contamination concentration.

4.2.5. Effect of QS-Fe/Pb dosage

The experiment that evaluate the dependence of the CIP and Cu(II) removal on the amount of QS-Fe/Pb dosage was done using prepared composite range from 0.05 to 1 g/50 mL. Each dosage was added and continuously mixed with 50 mL of aqueous contaminants solution at operating conditions clarified in Fig. 6E. The obtained results show that when 0.2 g/50 mL of QS-Fe/Pb composite was used, only 74% of the CIP and 60% of the Cu(II) were removed. However, an increase in the composite dosage to 0.5 and 0.7 g/50 mL for the CIP and Cu(II), respectively, might induce a large enhancement in the removal rate to 99% due to raised amounts of the sorbent material that provides more numbers of active sites [41,42]. It is also obvious that an increased dosage above 0.5 and 0.7 g/100 mL, respectively, of the CIP and Cu(II), does not considerably affect the percent removal duo to the stabilization of the contaminant concentration that remained in the aqueous phase. This finding agree with many researchers [23,43,44]. The maximum adsorption capacity of the prepared nanocomposite (QS-Fe/Pb) was estimated experimentally from the experiments of this section, which were 15 and 9.8 mg/g for CIP and Cu(II), respectively, these values are the highest compared to other materials that were used in previous works, as shown in Table 1. This indicates that

Table 1
Comparison of the adsorption capacity of QS-Fe/Pb nanocomposite with other adsorbent materials

Adsorbent material	Adsorption capacity		References
	Ciprofloxacin	Cu(II)	
Zero-valent iron (nZVI) with copper (Cu) bimetallic	0.5 mg/g		[15]
Clay-supported Fe/Ni		5 mg/g	[5]
Polyvinylpyrrolidone stabilized nZVI/Cu	1.16 mg/g		[16]
Green tea nano zero-valent iron (GT-nZVI)	9.9 mg/g		[2]
Bimetallic iron/nickel nanoparticles		0.2 mg/g	[8]
Zero-valent iron (nZVI) with magnesium hydroxide	1.6 mg/g		[1]
QS-Fe/Pb nanocomposite	15 mg/g		Current study
QS-Fe/Pb nanocomposite		9.8 mg/g	Current study

the nanocomposite (QS-Fe/Pb) has good adsorption capacity (efficient) in comparison with other materials.

4.3. Sorption isotherm

The sorption test results for the interaction of the QS-Fe/Pb with CIP and Cu(II) are described in terms of the equilibrium results by using the models of the adsorption isotherms previously described. A list of the parameters for these models is provided in Table 2. As can be seen in Fig. 7, the models were tested against the experimental data. Since the Freundlich model has a higher coefficient of determination (R^2) than the Langmuir model, it is obvious that it fits the data better and more accurately describes the sorption process. This suggests that CIP and Cu will bind to multi-molecular layers on the surface of the QS-Fe/Pb.

4.4. Sorption kinetic

As can be seen in Fig. 8, the pseudo-first-order and pseudo-second-order kinetic models were used to establish the kinetic models. Non-linear regression was used for kinetic models with experimental results using Microsoft Excel 2016. Table 2 displays a list of the kinetic model parameters, determination coefficients (R^2), and sum square error (SSE) values. This table demonstrates that the pseudo-second-order model, which also has the highest R^2 values and the lowest SSE values, is well adapted to the CIP and Cu(II) kinetic sorption data. Therefore, the sorption kinetic of the Cu(II) and CIP onto the prepared composite was chemisorption. Applying the intraparticle diffusion model to the measurements of the sorption kinetics revealed that the $t^{0.5}$ can relate to the qt in the linear relationships with an acceptable R^2, as shown in Fig. 9.

The lines in the intraparticle diffusion model that intersect with the y-axis at particular values demonstrate that intraparticle diffusion occurs in the CIP and Cu(II) sorbents despite the fact that this step is not rate-controlling. The three linearity sections are represented by the plotted lines as well, whereas there are usually two or more steps involved in the sorption. The rate constant (k), which represents the slopes of the plotted lines, has larger values for "part 1" than for "portions 2 and 3," as seen in Table 3. Hence, it is possible to regulate the first portion by prompt or external surface

Table 2
Parameters of the isotherm models

Model	Parameter	Ciprofloxacin	Cu(II)
Freundlich	K_F (mg/g)(L/mg)$^{1/n}$	4.508	2.27
	n	3.175	2.85
	R^2	0.984	0.967
	SSE	4.606	3.874
Langmuir	q_m (mg/g)	14.740	8.700
	b (L/mg)	0.290	0.120
	R^2	0.932	0.960
	SSE	22.986	7.482

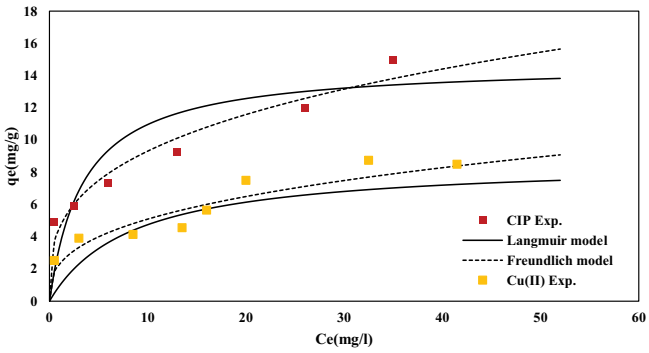

Fig. 7. Concurrence between equilibrium isotherms and sorption measurements for ciprofloxacin and Cu(II).

sorption. The rate constant (k), which represents the slopes of the plotted lines, has higher values for "portion 1" than for "portions 2 and 3," as shown in Table 3. As a result, the first portion can be controlled by instantaneous or external surface sorption [45]. According to the data obtained, it appears that there are three main steps in the sorption processes of CIP and Cu(II) on the QS-Fe/Pb composite, indicating that intraparticle diffusion is not the reaction's limiting factor overall. The first step (portion 1) is bulk diffusion, the second (portion 2) is the linear phase, represented by intraparticle diffusion, and the final step is equilibrium (portion 3). The slopes of the straight lines are used to determine the values

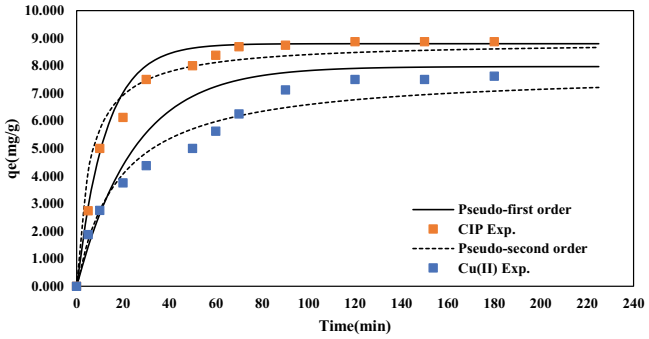

Fig. 8. Kinetic models and experimental measurements for sorption of ciprofloxacin and Cu(II).

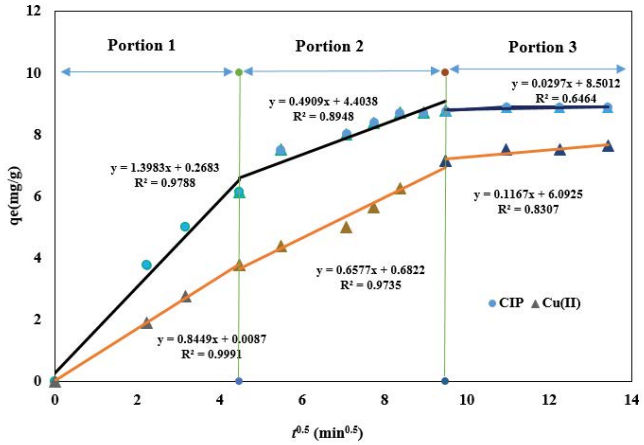

Fig. 9. Intraparticle diffusion model and experimental measurements for sorption of ciprofloxacin and Cu(II).

of K_1, K_2, and K_3 as shown in Table 3. Because the macro pore diffusion was greater than the micro pore diffusion, it was hypothesized that the diffusion of the pores and film played a significant role in the sorbent [46]. Microsoft Excel was used to calculate the parameters of the models using linear regression [47]. Because the lines did not pass at the origin point, diffusion controlled the rate while external mass transfer governed the sorption process for the contaminants [48].

4.5. Reusability of QS-Fe/Pb

The reusability test was carried out by repeatedly interacting QS-Fe/Pb that had already undergone reaction with CIP and Cu(II) solution for 5 cycles, the highest removal percentage (99%) was attained under optimal conditions from previous steps. With each reuse cycle, from the first to the fifth, the removal % gradually decreased, as can be shown in Fig. 10. Moreover, to confirm the strongly bonded of the Fe/Pb nanoparticles to the sand surface, the Fe and Pb ion was analyzed in the aqueous solution after all five cycles of reuse. The findings demonstrated that the concentration of the leached Fe ions was minimal even after the fifth cycle, while the Pb leaching was below 18 g/L at the conclusion of the fifth cycle, indicating little leaching of Fe/Pb out of the sand to the aqueous solutions following reaction with CIP

Table 3
Parameters of kinetic models for sorption of ciprofloxacin and Cu(II)

Kinetic	Parameter	Ciprofloxacin	Cu(II)
Pseudo-first-order	q_e (mg/g)	8.800	7.970
	$q_{e,exp}$ (mg/g)	8.875	7.625
	K_1 (min^{-1})	0.080	0.040
	R^2	0.97	0.96
	SSE	2.361	10.644
Pseudo-second-order	$q_{e,exp}$ (mg/g)	8.875	7.625
	q_e (mg/g)	8.880	7.800
	K_2 (g/mg·min)	0.020	0.007
	R^2	0.987	0.973
	SSE	2.058	2.544
Intraparticle diffusion	Portion 1		
	k_{int} (mg/g·$min^{0.5}$)	1.3983	0.8449
	R^2	0.9788	0.9991
	Portion 2		
	k_{int} (mg/g·$min^{0.5}$)	0.4909	0.6577
	R^2	0.8948	0.9735
	Portion 3		
	k_{int} (mg/g·$min^{0.5}$)	0.0297	0.1167
	R^2	0.6464	0.8307

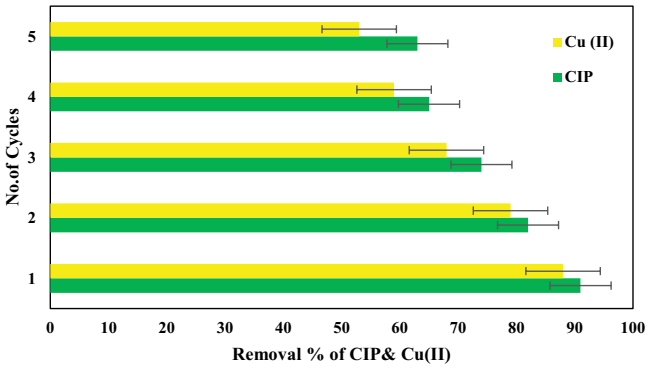

Fig. 10. Reusability of QS-Fe/Pb for removal of ciprofloxacin and Cu(II) for many cycles.

and Cu(II), this confirms the strong bonding between sand and nanoparticles (Fe/Pb). Based on the information provided above, creating the bimetallic nanoparticles on sand can be done in an extremely profitable and environmentally responsible manner.

5. Conclusion

QS-Fe/Pb composite was synthesized using a simple green method. This process is free from any toxic chemicals, which might have adverse side effects on the environment, for reducing Fe/Pb. The prepared composite showed removal capability for organic (CIP) and inorganic Cu(II) contaminants using batch processes. The investigated parameters, that influenced the removal of CIP and Cu(II),

included the contact time, initial pH, agitation speed, initial concentration, and QS-Fe/Pb composite dosage, the effective values of these parameters were (70 min, 7, 200 rpm, 50 mg/L, and 0.5 g/50 mL) for CIP, and (120 min, 6, 200 rpm, 50 mg/L, 0.7 g/50 mL for Cu(II)), at which the maximum removal percent for CIP and Cu(II) was 99%. The experimental batch results proved that the sorption data for CIP and Cu(II) were better represented by the Freundlich isotherm model suggested multi-molecular layer sorption. Also, from a kinetics perception, the pseudo-second-order model fitted the experimental data, so, the kinetics of sorption of the CIP and Cu(II) was chemisorption, in addition, The intraparticle diffusion model demonstrated that the external mass transfer controlled the sorption process while diffusion controlled the rate. Finally, The results propose a possible green means to synthesize a bimetallic nano-material on the sand and its effective utilization for CIP and Cu(II) removal from aqueous solutions.

References

[1] O. Falyouna, I. Maamoun, K. Bensaida, A. Tahara, Y. Sugihara, O. Eljamal, Encapsulation of iron nanoparticles with magnesium hydroxide shell for remarkable removal of ciprofloxacin from contaminated water, J. Colloid Interface Sci., 605 (2022) 813–827.

[2] M.A. Atiya, A.K. Hassan, F.Q. Kadhim, Green synthesis of iron nanoparticle using tea leave extract for removal ciprofloxacin (CIP) from aqueous medium, J. Eng. Sci. Technol., 16 (2021) 3199–3221.

[3] Z.T. Abd Ali, H.J. Khadim, M.A. Ibrahim, Simulation of the remediation of groundwater contaminated with ciprofloxacin using grafted concrete demolition wastes by ATPES as reactive material: batch and modeling study, Egypt. J. Chem., 65 (2022) 585–596.

[4] D.J. Lapworth, N. Baran, M.E. Stuart, R.S. Ward, Emerging organic contaminants in groundwater: a review of sources, fate and occurrence, Environ. Pollut., 163 (2012) 287–303.

[5] G. Gopal, C. Natarajan, A. Mukherjee, Synergistic removal of tetracycline and copper(II) by *in-situ* B-Fe/Ni nanocomposite—a novel and an environmentally sustainable green nanomaterial, Environ. Technol. Innovation, 25 (2022) 102187, doi: 10.1016/j.eti.2021.102187.

[6] Z.T. Abd Ali, Using activated carbon developed from iraqi date palm seeds as permeable reactive barrier for remediation of groundwater contaminated with copper, Al-Khwarizmi Eng. J., 12 (2016) 34–44.

[7] Z.T. Abd Ali, Green synthesis of graphene-coated sand (GCS) using low-grade dates for evaluation and modeling of the pH-dependent permeable barrier for remediation of groundwater contaminated with copper, Sep. Sci. Technol., 56 (2021) 14–25.

[8] Y. Lin, X. Jin, G. Owens, Z. Chen, Simultaneous removal of mixed contaminants triclosan and copper by green synthesized bimetallic iron/nickel nanoparticles, Sci. Total Environ., 695 (2019) 133878, doi: 10.1016/j.scitotenv.2019.133878.

[9] Q. Qin, X. Wu, L. Chen, Z. Jiang, Y. Xu, Simultaneous removal of tetracycline and Cu(II) by adsorption and coadsorption using oxidized activated carbon, RSC Adv., 8 (2018) 1744–1752.

[10] T.A. Saleh, I. Ali, Synthesis of polyamide grafted carbon microspheres for removal of rhodamine B dye and heavy metals, J. Environ. Chem. Eng., 6 (2018) 5361–5368.

[11] A.A. Basaleh, M.H. Al-Malack, T.A. Saleh, Poly(acrylamide acrylic acid) grafted on steel slag as an efficient magnetic adsorbent for cationic and anionic dyes, J. Environ. Chem. Eng., 9 (2021) 105126, doi: 10.1016/j.jece.2021.105126.

[12] O. Al-Hashimi, K. Hashim, E. Loffill, T. Marolt Čebašek, I. Nakouti, A.A.H. Faisal, N. Al-Ansari, A comprehensive review for groundwater contamination and remediation: occurrence, migration and adsorption modelling, Molecules, 26 (2021) 5913, doi: 10.3390/molecules26195913.

[13] M. Stefaniuk, P. Oleszczuk, Y.S. Ok, Review on nano zero-valent iron (nZVI): from synthesis to environmental applications, Chem. Eng. J., 287 (2016) 618–632.

[14] R.A. Crane, T.B. Scott, Nanoscale zero-valent iron: future prospects for an emerging water treatment technology, J. Hazard. Mater., 211 (2012) 112–125.

[15] L. Chen, R. Ni, T. Yuan, Y. Gao, W. Kong, P. Zhang, Q. Yue, B. Gao, Effects of green synthesis, magnetization, and regeneration on ciprofloxacin removal by bimetallic nZVI/Cu composites and insights of degradation mechanism, J. Hazard. Mater., 382 (2020) 121008, doi: 10.1016/j.jhazmat.2019.121008.

[16] L. Chen, T. Yuan, R. Ni, Q. Yue, B. Gao, Multivariate optimization of ciprofloxacin removal by polyvinylpyrrolidone stabilized nZVI/Cu bimetallic particles, Chem. Eng. J., 365 (2019) 183–192.

[17] G. Gopal, H. Sankar, C. Natarajan, A. Mukherjee, Tetracycline removal using green synthesized bimetallic nZVI-Cu and bentonite supported green nZVI-Cu nanocomposite: a comparative study, J. Environ. Manage., 254 (2020) 109812, doi: 10.1016/j.jenvman.2019.109812.

[18] K.V.G. Ravikumar, S.V. Sudakaran, K. Ravichandran, M. Pulimi, C. Natarajan, A. Mukherjee, Green synthesis of NiFe nano particles using *Punica granatum* peel extract for tetracycline removal, J. Cleaner Prod., 210 (2019) 767–776.

[19] X. Weng, Q. Sun, S. Lin, Z. Chen, M. Megharaj, R. Naidu, Enhancement of catalytic degradation of amoxicillin in aqueous solution using clay-supported bimetallic Fe/Ni nanoparticles, Chemosphere, 103 (2014) 80–85.

[20] Z. Chen, X. Jin, Z. Chen, M. Megharaj, R. Naidu, Removal of methyl orange from aqueous solution using bentonite-supported nanoscale zero-valent iron, J. Colloid Interface Sci., 363 (2011) 601–607.

[21] X. Weng, W. Cai, R. Lan, Q. Sun, Z. Chen, Simultaneous removal of amoxicillin, ampicillin and penicillin by clay-supported Fe/Ni bimetallic nanoparticles, Environ. Pollut., 236 (2018) 562–569.

[22] Y. Li, C. Guo, J. Yang, J. Wei, J. Xu, S. Cheng, Evaluation of antioxidant properties of pomegranate peel extract in comparison with pomegranate pulp extract, Food Chem., 96 (2006) 254–260.

[23] K.V.G. Ravikumar, G. Debayan, P. Mrudula, N. Chandrasekaran, M. Amitava, *In-situ* formation of bimetallic FeNi nanoparticles on sand through green technology: application for tetracycline removal, Front. Environ. Sci. Eng., 14 (2020) 1–13.

[24] B.H. Graimed, Z.T. Abd Ali, Green approach for the synthesis of graphene glass hybrid as a reactive barrier for remediation of groundwater contaminated with lead and tetracycline, Environ. Nanotechnol. Monit. Manage., 18 (2022) 100685, doi: 10.1016/j.enmm.2022.100685.

[25] A.F. Ali, Z.T. Abd Ali, Sustainable use of concrete demolition waste as reactive material in permeable barrier for remediation of groundwater: batch and continuous study, J. Environ. Eng., 146 (2020) 4020048, doi: 10.1061/(ASCE)EE.1943-7870.0001714.

[26] N. Saad, Z.T. Abd Ali, L.A. Naji, A.A.A.H. Faisal, N. Al-Ansari, Development of Bi-Langmuir model on the sorption of cadmium onto waste foundry sand: effects of initial pH and temperature, Environ. Eng. Res., 25 (2020) 677–684.

[27] Z.T. Abd Ali, H.M. Flayeh, M.A. Ibrahim, Numerical modeling of performance of olive seeds as permeable reactive barrier for containment of copper from contaminated groundwater, Desal. Water Treat., 139 (2019) 268–276.

[28] A.F. Ali, Z.T. Abd Ali, Interaction of aqueous Cu^{2+} ions with granules of crushed concrete, Iraqi J. Chem. Pet. Eng., 20 (2019) 31–38.

[29] Z.T. Abd Ali, A comparative isothermal and kinetic study of the adsorption of lead(II) from solution by activated carbon and bentonite, J. Eng., 21 (2015) 45–58.

[30] A.A.H. Faisal, Z.T. Abd Ali, Groundwater protection from lead contamination using granular dead anaerobic sludge biosorbent as permeable reactive barrier, Desal. Water Treat., 57 (2016) 3891–3903.

[31] Z.T. Abd Ali, Z.Z. Ismail, Experimental and modeling study of water defluoridation using waste granular brick in a

continuous up-flow fixed bed, Environ. Eng. Res., 26 (2021) 190506, doi: 10.4491/eer.2019.506.
[32] L. Du, L. Luo, Z. Feng, M. Engelhard, X. Xie, B. Han, J. Sun, J. Zhang, G. Yin, C. Wang, Nitrogen–doped graphitized carbon shell encapsulated NiFe nanoparticles: a highly durable oxygen evolution catalyst, Nano Energy, 39 (2017) 245–252.
[33] Z.-J. Li, L. Wang, L.-Y. Yuan, C.-L. Xiao, L. Mei, L.-R. Zheng, J. Zhang, J.-H. Yang, Y.-L. Zhao, Z.-T. Zhu, Efficient removal of uranium from aqueous solution by zero-valent iron nanoparticle and its graphene composite, J. Hazard. Mater., 290 (2015) 26–33.
[34] S. Kaviya, Rapid naked eye detection of arginine by pomegranate peel extract stabilized gold nanoparticles, J. King Saud Univ., 31 (2019) 864–868.
[35] A.M. Osman, A.H. Hendi, T.A. Saleh, Simultaneous adsorption of dye and toxic metal ions using an interfacially polymerized silica/polyamide nanocomposite: kinetic and thermodynamic studies, J. Mol. Liq., 314 (2020) 113640, doi: 10.1016/j.molliq.2020.113640.
[36] J. Liu, Y. Du, W. Sun, Q. Chang, C. Peng, A granular adsorbent-supported Fe/Ni nanoparticles activating persulfate system for simultaneous adsorption and degradation of ciprofloxacin, Chin. J. Chem. Eng., 28 (2020) 1077–1084.
[37] D. Wang, J. Li, Z. Xu, Y. Zhu, G. Chen, Preparation of novel flower-like $BiVO_4/Bi_2Ti_2O_7/Fe_3O_4$ for simultaneous removal of tetracycline and Cu^{2+}: adsorption and photocatalytic mechanisms, J. Colloid Interface Sci., 533 (2019) 344–357.
[38] Z.T. Abd Ali, Green synthesis of graphene-coated glass as novel reactive material for remediation of fluoride-contaminated groundwater, Desal. Water Treat., 226 (2021) 113–124.
[39] Z.T. Abd Ali, L.A. Naji, S.A. Almuktar, A.A.H. Faisal, S.N. Abed, M. Scholz, Mu. Naushad, T. Ahamad, Predominant mechanisms for the removal of nickel metal ion from aqueous solution using cement kiln dust, J. Water Process Eng., 33 (2020) 101033, doi: 10.1016/j.jwpe.2019.101033.
[40] M.N. Ezzat, Z.T. Abd Ali, Green approach for fabrication of graphene from polyethylene terephthalate (PET) bottle waste as reactive material for dyes removal from aqueous solution: batch and continuous study, Sustainable Mater. Technol., 32 (2022) e00404, doi: 10.1016/j.susmat.2022.e00404.
[41] G. Lamzougui, A. Es-Said, H. Nafai, D. Chafik, A. Bouhaouss, R. Bchitou, Optimization and modeling of Pb(II) adsorption from aqueous solution onto phosphogypsum by application of response surface methodology, Phosphorus, Sulfur Silicon Relat. Elem., 196 (2021) 521–529.
[42] B.H. Graimed, Z.T. Abd Ali, Batch and continuous study of one-step sustainable green graphene sand hybrid synthesized from date-syrup for remediation of contaminated groundwater, Alexandria Eng. J., 61 (2022) 8777–8796.
[43] J. Jin, Z. Yang, W. Xiong, Y. Zhou, R. Xu, Y. Zhang, J. Cao, X. Li, C. Zhou, Cu and Co nanoparticles co-doped MIL-101 as a novel adsorbent for efficient removal of tetracycline from aqueous solutions, Sci. Total Environ., 650 (2019) 408–418.
[44] S. Kango, R. Kumar, Magnetite nanoparticles coated sand for arsenic removal from drinking water, Environ. Earth Sci., 75 (2016) 1–12.
[45] Z.T. Abd Ali, Combination of the artificial neural network and advection-dispersion equation for modeling of methylene blue dye removal from aqueous solution using olive stones as reactive bed, Desal. Water Treat., 179 (2020) 302–311.
[46] A.A.H. Faisal, Z.T. Abd Ali, Remediation of groundwater contaminated with the lead–phenol binary system by granular dead anaerobic sludge-permeable reactive barrier, Environ. Technol., 38 (2017) 2534–2542.
[47] Z.B. Masood, Z.T.A. Ali, Numerical modeling of two-dimensional simulation of groundwater protection from lead using different sorbents in permeable barriers, Environ. Eng. Res., 25 (2020) 605–613.
[48] T.H. Mhawesh, Z.T. Abd Ali, Reuse of brick waste as a cheap-sorbent for the removal of nickel ions from aqueous solutions, Iraqi J. Chem. Pet. Eng., 21 (2020) 15–23.